

Extreme sensitivity of graphene photoconductivity to environmental gases

Callum J. Docherty,¹ Cheng-Te Lin,² Hannah J. Joyce,¹ Robin J. Nicholas,¹ Laura M. Herz,¹ Lain-Jong Li,² and Michael B. Johnston^{1,*}

¹*Clarendon Laboratory, Department of Physics, University of Oxford, Oxford, OX1 3PU, UK*

²*Institute of Atomic and Molecular Sciences, Academia Sinica, Taipei, 10617, Taiwan*

Graphene is a single layer of covalently bonded carbon atoms that was discovered only eight years ago and yet has already attracted intense research and commercial interest. Initial research focused on its remarkable electronic properties, such as the observation of massless Dirac Fermions and the half-integer quantum Hall effect. Now, graphene is finding application in touch-screen displays, as channels in high-frequency transistors, and in graphene-based integrated circuits. The potential for using the unique properties of graphene in terahertz-frequency electronics is particularly exciting, however initial experiments probing the terahertz frequency response of graphene are only just emerging. Here we show that the photoconductivity of graphene at terahertz frequencies is dramatically altered by the adsorption of atmospheric gases, such as nitrogen and oxygen. Furthermore, we observe the signature of terahertz stimulated emission from gas-adsorbed graphene. Our findings highlight the importance of environmental conditions on the design and fabrication of high-speed graphene-based devices.

PACS numbers: **Open source version of this article is available at Nature Communications DOI: 10.1038/ncomms2235**

The experimental realisation of graphene, a single layer of graphite, in 2004 [1] rapidly led to the observation of massless Dirac fermions and the half-integer quantum Hall effect[2]. Since then many potential applications have been suggested[3, 4], and recently graphene-based touch-screen displays[5], transistors[6, 7], and integrated circuits[8] have been demonstrated. The high mobility of charge carriers in graphene makes it an ideal material for extremely high-speed devices[6, 7], indeed terahertz frequency switching has been predicted[3]. The potential for the realisation of such devices was greatly enhanced by the emergence of large area graphene sheets grown by chemical vapour deposition (CVD) [9]. However, the design and production of these high-frequency devices requires a fuller understanding of both nonequilibrium carrier dynamics in graphene [10], and its susceptibility to environmental conditions [11].

Ultrafast spectroscopic techniques provide an excellent probe of non-equilibrium carrier dynamics in graphene[12]. Ultrafast cooling and relaxation of photoexcited charge carriers in graphene have been observed using optical pump–optical probe spectroscopy. Several studies [10, 13, 14] have shown that graphene becomes more transparent at optical frequencies after intense photoexcitation (photoinduced bleaching), owing to state blocking of interband absorption. Furthermore these studies showed that thermalisation of photoexcited carriers occurs within tens of femtoseconds, and a subsequent cooling by carrier–phonon interactions occurs on a picosecond timescale.

While optical photons probe interband charge dynamics, terahertz frequency photons are excellent probes of intraband dynamics. Studies of intraband relaxation in graphene have been performed using optical pump–terahertz probe spectroscopy (OPTPS) [12, 15–17]. George et al.[15] revealed that the absorption of the terahertz photons in epitaxially grown graphene increases after intense (interband) optical excitation. The increase in absorption was attributed to an increase in the density of mobile charge carriers after photoexcitation. However, a comparable study on chemical vapour deposition (CVD) grown graphene found the opposite effect, photoinduced bleaching [18]. It is known that CVD grown graphene is p-doped, due to residual impurities and defects from the production process [19], unlike epitaxial graphene [17]. Despite this, equilibrium carrier dynamics in CVD grown graphene have been shown to be similar to other forms of graphene in the terahertz regime, suggesting that growth conditions cannot explain the discrepancy between the epitaxial and CVD graphene in pump–probe studies [20].

In this study, we utilised terahertz time domain spectroscopy to measure the photoconductivity of CVD grown graphene in four different environment types: air, oxygen, nitrogen and vacuum. We demonstrate that CVD grown graphene can display either photoinduced bleaching or photoinduced absorption depending on the type and density of gas adsorbed on its surface. Our results highlight the dramatic effects environmental conditions have on the high-frequency electrical properties of graphene. These results have important implications for the design of future graphene electronic devices. In particular, the order-of-magnitude changes in photoconductivity we observe could provide a basis for precise graphene based gas monitors. Conversely, the sensitivity of the optoelectronic properties of graphene to environ-

*Electronic address: m.johnston@physics.ox.ac.uk

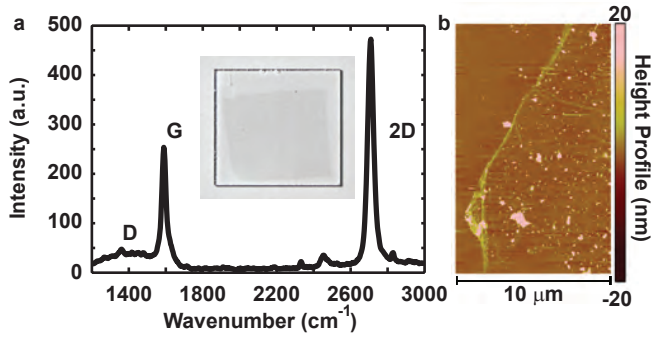


FIG. 1: Characterisation of graphene samples. **a** Raman spectroscopy. The relative intensities of the 2D and G peaks suggest monolayer graphene [21]. **Inset** Photograph of graphene sheet with area of $1 \times 1 \text{ cm}^2$ on quartz. **b** Surface topography of CVD-grown graphene measured by AFM. The residuals remaining on graphene surface can be attributed to incomplete decomposition or carbonization of PMMA.

mental conditions will need to be addressed during the design and fabrication of future devices.

Results

Sample preparation and characterisation

The CVD samples used in this study were grown on copper foil, and transferred to z-cut quartz substrates using poly(methyl methacrylate) as a supporting layer (for details see the Methods section). Raman microscopy and atomic force microscopy (AFM) revealed that the samples were primarily a graphene monolayer with relatively few defects. A typical Raman spectrum is shown in Figure 1 and exhibits a Lorentzian 2D Raman peak (2700 cm^{-1}), with the ratio of intensities of the 2D and G (1580 cm^{-1}) peaks, $I_{2D}/I_G \approx 2$, which is indicative of monolayer growth. Additionally, the relative weakness of the D peak (1350 cm^{-1}) demonstrates the small number of defects and low disorder in the samples, confirming their high quality [21]. UV-visible absorption measurements revealed an absorption of $\sim \pi\alpha$, where α is the fine structure constant, also suggesting monolayer growth (see Supplementary Methods) [22]. AFM images (Figure 1b) showed the graphene sheet thickness measured from the edge to be $\sim 0.72 \text{ nm}$, further suggesting monolayer growth [23]. Hall measurements revealed the sample to be p-doped, with hole density $8 \times 10^{12} \text{ cm}^{-2}$, and Fermi level $\varepsilon_F \sim -0.3 \text{ eV}$.

Terahertz time domain spectroscopy

In order to assess the influence of atmospheric gas adsorption on graphene we utilised terahertz spectroscopy. This technique allowed us to observe intraband charge

dynamics and investigate the high-frequency electrical properties of graphene. Terahertz spectroscopy is ideal for electrically characterising surface sensitive materials such as graphene as it is a non-contact technique, and covers an important frequency range ($\sim 100 \text{ GHz} - >3 \text{ THz}$) for high speed device operation[24]. OPTPS measurements were performed with CVD-grown graphene samples in an atmosphere of air, N_2 or O_2 , or in a vacuum. Before each set of measurements, the sample was left under a vacuum of 10^{-5} mbar for two hours, to remove existing adsorbants (see Supplementary Methods for Langmuir coverage calculations). For the vacuum measurements, the graphene was left for a further two hours with 800 nm (1.55 eV) “pump” photons incident upon the sample before measurement. For the gaseous measurements, 1 bar of air, N_2 or O_2 was introduced after two hours under vacuum, and measurements were taken after a further two hours, again with the “pump” beam incident upon the sample. Measurements were found to be reproducible on different samples and were independent of sample history. That is, the effect of exposure to any of the gases could be “reset” by placing the sample in vacuum for 2 hours.

For the measurements, the electric field of a terahertz pulse transmitted through the graphene was sampled after photoexcitation by an 800 nm , $180 \mu\text{J}/\text{cm}^2$ fluence pump pulse, $E_{\text{THz}}^{\text{ON}}$, and without the photoexcitation, $E_{\text{THz}}^{\text{OFF}}$. The photoinduced change in terahertz transmission of the sample, $\Delta E = E_{\text{THz}}^{\text{ON}} - E_{\text{THz}}^{\text{OFF}}$ was recorded using lock-in detection. The principle of the measurements is illustrated in Figure 2a. The terahertz pulse probes the photoexcited graphene sample at a time t_2 after photoexcitation. The terahertz probe is then mapped out in time by varying the difference in time of arrival, t_1 , between the terahertz pulse and an 800 nm gate pulse at an electro-optic detection crystal (GaP).

In Figures 2b and c we present the measured terahertz electric field, E_{THz} , transmitted through graphene in an pure oxygen atmosphere, and the corresponding change in transmission due to photoexcitation, ΔE . The induced ΔE decreases as the delay between pump and probe, t_2 , is increased. The photoinduced change in terahertz transmission is seen to decay within $\sim 5 \text{ ps}$. Further information may be extracted from these data by performing a Fourier transform on the electric field data to give directly the frequency dependent complex photoconductivity, $\Delta\sigma(\omega)$, without resorting to the Kramers-Kronig relations, via [17]

$$\Delta\sigma(\omega) = - \left(\frac{1 + n_s}{Z_0} \right) \frac{\Delta E(\omega)}{E_{\text{THz}}(\omega)}, \quad (1)$$

where Z_0 is the impedance of free space, $Z_0 = 377 \Omega$, and n_s is the refractive index of the quartz substrate, $n_r = 2.1$ [25] at terahertz frequencies. Figures 2d and e show the real and imaginary parts of the photoconductivity respectively as a function of pump-probe delay time.

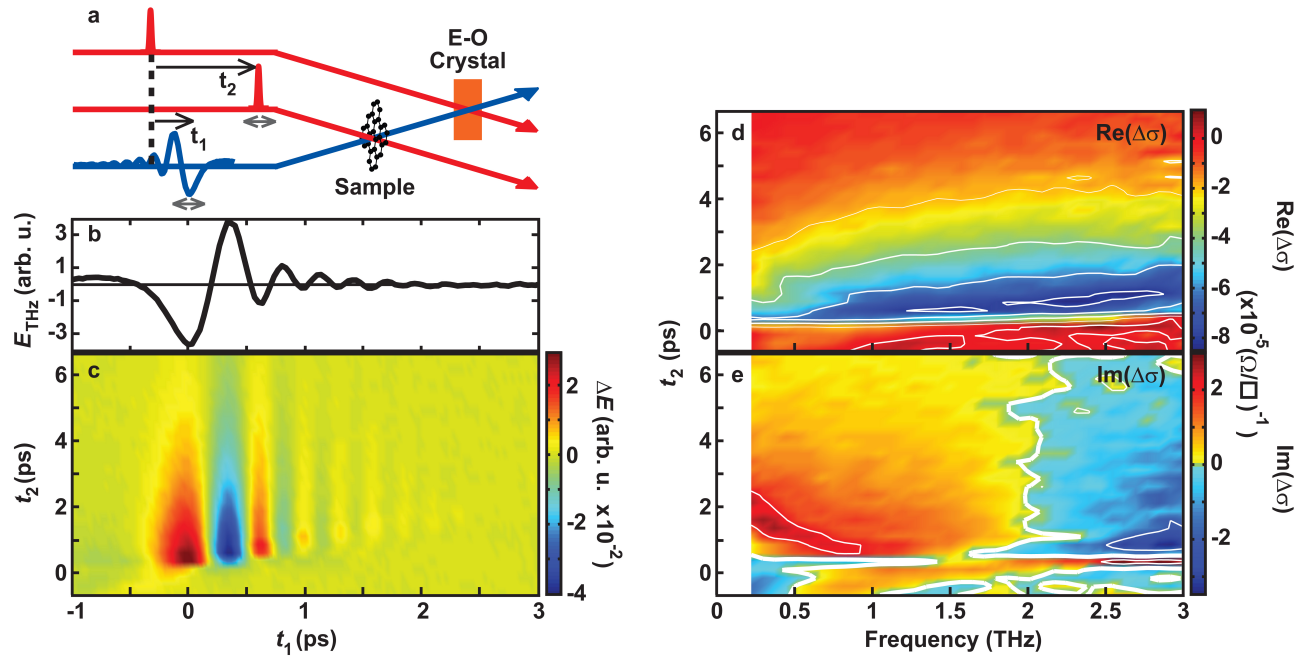


FIG. 2: Terahertz spectroscopy of graphene in O_2 . **a** Schematic representation of the measurement. Varying t_1 allows the electric field, E_{THz} , of the terahertz probe pulse to be sampled in the electro-optic (E-O) crystal. The sample can be probed at different times after photoexcitation by altering t_2 . **b,c** terahertz electric field, E_{THz} , transmitted through the sample (**b**), and the corresponding photoinduced change in transmission, ΔE (**c**), as a function of pump-probe delay time, t_2 . **d,e** Real (**d**) and imaginary (**e**) parts of the frequency dependent photoconductivity as a function of t_2 . The contours highlight increments of $2 \times 10^{-5} \text{ S}\square$. The thicker contour in **e** represents $\text{Im}(\Delta\sigma) = 0$, corresponding to the Lorentzian peak frequency, ω_0 .

To more easily compare the photoconductivity in different atmospheres, we take slices of the data from Figure 2, and the corresponding data for the other environment types. For instance, holding t_1 constant at the maximum terahertz electric field (e.g. $t_1=0$ in Figure 2c) and observing the resulting ΔE as pump-probe delay time t_2 is varied, yields an optical pump-terahertz probe measurement, which provides the average terahertz response of the sample. In Figure 3, we plot $-\Delta E/E_{\text{THz}}$, which is proportional to the photoconductivity of the graphene, as a function of the delay time between the pump and probe pulses in the four atmosphere types. It should be noted that due to the large number of holes already present near the Dirac point in this p doped sample, the transient response probed by the terahertz is dominated by electron dynamics.

Immediately after photoexcitation in vacuum, the terahertz conductivity increases (photoinduced absorption) within 1 ps, and subsequently relaxes with two distinct time scales. Initially fast cooling occurs within ~ 0.6 ps, and a longer, exponential cooling occurs with a time scale of ~ 2.5 ps. Such a relaxation is consistent with other studies, which associated the first rapid cooling with emission of optical phonons, followed by a bottleneck when the carrier temperature cools below the hot optical phonon temperature (~ 0.196 and 0.162 eV [16]), slowing further cooling [10, 14, 16].

However, when graphene is placed in a gaseous atmo-

sphere, the photoinduced change is dramatically different. Surprisingly, the photoconductivity signal flips from being purely positive in vacuum to purely negative in all the gas environments. Following photoexcitation in air, N_2 or O_2 , the terahertz conductivity decreases within 1 ps, and then relaxes with a common monoexponential time scale of 2.5 ps. The similarity between this time constant and that of cooling in vacuum suggests the continued importance of carrier-phonon interactions. Adsorbed O_2 was found to have the strongest influence on charge dynamics in graphene, with the negative photoconductivity almost an order of magnitude greater than the induced absorption under vacuum. A negative transient absorption, such as we observe, may be attributed to either stimulated emission in the samples or a bleaching effect. To understand more about the origin of the negative photoconductivity it is informative to consider the photoconductivity spectra at a fixed time after photoexcitation.

Figure 4 shows the photoconductivity in all four atmosphere types at 2 ps after photoexcitation ($t_2 = 2$ ps). The spectrum of graphene in vacuum reveals a relatively flat and positive real part of photoconductivity, in stark contrast to the strongly negative (real) photoconductivity seen for gas-absorbed graphene. Furthermore the spectral photoconductivity of graphene samples in the presence of N_2 , air and O_2 can be seen to exhibit a

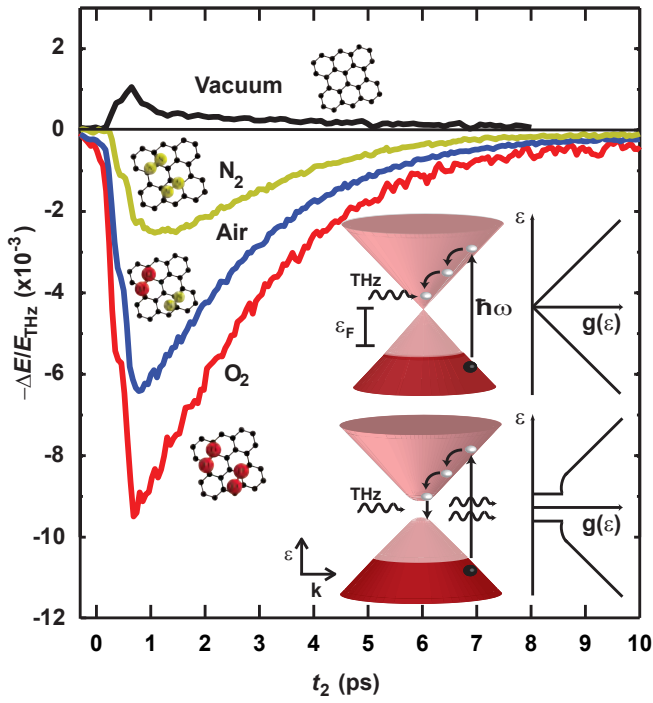


FIG. 3: Environmental dependence of pump induced change in terahertz photoconductivity, $-\Delta E/E_{\text{THz}}$. Here, $\Delta E = E_{\text{THz}}^{\text{ON}} - E_{\text{THz}}^{\text{OFF}}$. From top to bottom: graphene in vacuum, N_2 , air and O_2 . Photoinduced absorption is observed in vacuum, but photoinduced bleaching is observed in gaseous environments. Inset: Schematic representation of the pump-probe measurements of p-doped graphene ($\varepsilon_{\text{F}} \sim -0.3 \text{ eV}$) in vacuum (top), and in the presence of gases (bottom), with corresponding density of states ($g(\varepsilon)$). The high energy pump ($\hbar\omega$) excites carriers far above the Dirac point, which cool by phonon emission. In gapless graphene, terahertz photons can be absorbed by the photoexcited carriers. In the presence of gases, stimulated emission releases extra terahertz photons, yielding a bleaching pump-probe signal.

Lorentzian form,

$$\sigma_{\text{Lorentz}} \propto \frac{i\omega}{\omega^2 - \omega_0^2 + i\omega\Gamma}, \quad (2)$$

where Γ is the linewidth, and ω_0 is the resonant frequency. The solid lines in Figure 4 represent a least square fit of Eq. 2 to the experimental data. The fitted resonant frequency for graphene in air and N_2 was found to be $\omega_0 \sim 1.8 \text{ THz}$, compared with $\omega_0 \sim 2 \text{ THz}$ for graphene in an O_2 environment. The resonance in all gas types is spectrally very broad; the fitted linewidth was $\Gamma \approx 10 \text{ THz}$, independent of the gas type. The Lorentzian fit begins to deviate from the measured photoconductivity at low frequencies. The deviation is most noticeable for O_2 -exposed graphene (Figure 4d). The non-zero value of $\text{Re}(\Delta\sigma)$ evident in the data at low frequency suggests an underlying Drude-like response, however inclusion of a Drude term does not enhance the fit within our observable bandwidth, so has been neglected. In con-

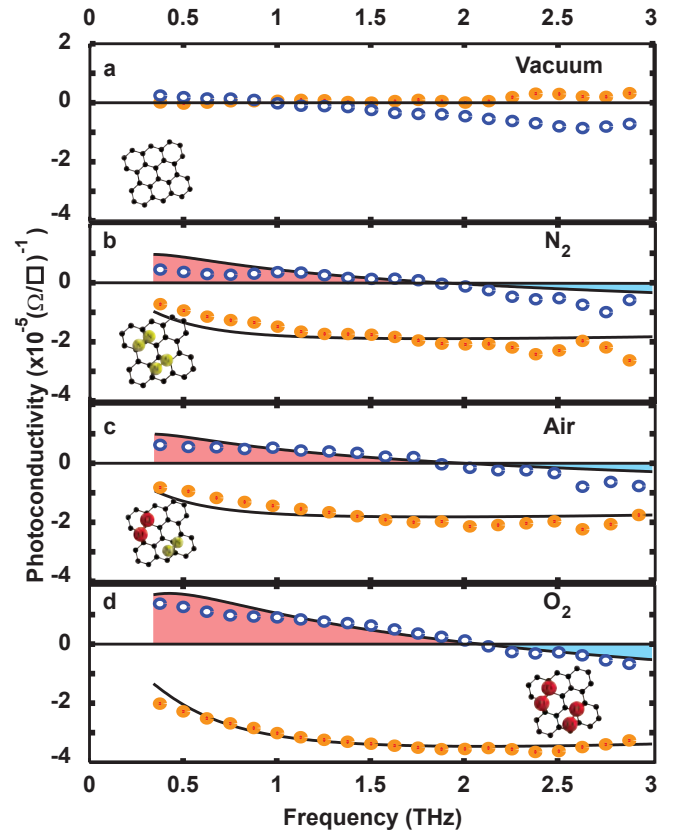


FIG. 4: Photoconductivity spectra of graphene in different environments. **a-d** Photoconductivity in vacuum (**a**), N_2 (**b**), air (**c**) and O_2 (**d**), taken at 2 ps after photoexcitation by the optical pump. Solid orange dots show the real part of the photoconductivity, hollow blue dots show the imaginary part. The solid black line in **b-d** is a Lorentzian model fit to the conductivity data, demonstrating the Lorentzian form of the photoconductivity in gaseous environments. Shading is used to emphasise the change from positive to negative $\text{Im}(\Delta\sigma)$. This point corresponds to the peak Lorentzian frequency, ω_0 .

trast, the photoinduced absorption in vacuum leads to a small, positive, spectrally flat real conductivity, with a non-negligible imaginary part.

A negative transient absorption signal with a Lorentzian lineshape is characteristic of stimulated emission. Hence, our data provide evidence that stimulated emission of terahertz photons is occurring in photoexcited graphene in the presence of atmospheric gases. Theoretical studies have predicted amplified stimulated emission of terahertz radiation from sufficiently intensely photoexcited graphene[26]. The proposed mechanism is that after photoexcitation, the charge carriers relax and populate states around the Dirac point, from where they can radiatively recombine. Thus terahertz emission over a large spectral range is expected to be possible[26]. Whilst our measurements do not show amplification of the terahertz probe (losses are still greater than gain), stimulated terahertz emission, below the gain threshold is consistent with our observations.

Discussion

We now consider the mechanism for the dramatic changes of photoconductivity in graphene under the different gas environments. The ability to “reset” the effects of gas exposure by placing the graphene samples in vacuum for two hours (at room temperature) suggests that the gas molecules are physisorbed rather than chemisorbed to the graphene surface. Physisorption of O₂ and N₂ on graphene could act as a dopant [27], lead to the opening of a small bandgap at the Dirac point [28, 29], and/or lead to a modification of the density of states [30, 31]. Hall measurements (see Methods) showed only 3% changes in the Fermi level after gas adsorption, indicating that doping alone is unlikely to account for the huge change in photoconductivity we observe. The opening of a ~ 8 meV bandgap upon gas adsorption, and associated increase in the density of electron and hole states near the band extrema would be consistent with our observations. In this case, electrons injected into the conduction band by 800 nm (1.55 eV) photoexcitation would relax rapidly to near the band minimum via phonon mediated processes, as shown on the inset of Figure 3. Recombination for the photoinjected electrons across the bandgap with a sea of holes would lead to the observed stimulated emission signal. The spectral broadness ($\Gamma \approx 10$ THz) of the observed transition may then be explained by a combination of the following factors: a high interband transition rate (lifetime broadening), fast dephasing via electron-electron interactions and a cooling bottleneck below the optical phonon energies. However full *ab-initio* calculations would be required to confirm the exact mechanism. Note that since CVD graphene is heavily p-doped, the opening of a bandgap is not directly observable by terahertz transmission spectroscopy, as there are no electrons near the band gap to be excited by the low energy terahertz photons (see Supplementary Discussion and inset of Figure 3).

The adsorption of molecules on graphene would locally open a bandgap and hence alter the otherwise linear density of states ($g(\varepsilon)$) of the graphene, thereby increasing $g(\varepsilon)$ at the top of the valance band and bottom of the conduction band (see inset of Figure 3) [31]. However, a gap would only be opened in regions around adsorbed gas molecules, creating islands of semiconducting graphene amongst the unaltered, gapless graphene (see Supplementary Methods for Langmuir coverage calculations). As the terahertz probe is much larger than these puddles, the observed photoconductivity behaviour is the result of an interaction with of both types of graphene. Increased stimulated emission will therefore be observed if gas molecules are more effectively adsorbed on the surface, thus creating a higher proportion of semiconducting material. Of the gases used in this study, O₂ is most likely to interact with graphene [32, 33], which is consistent with the increased negative photoconductivity signal observed in pure O₂ compared with air and N₂.

There are a number of other possible explanations for

a Lorentzian photoconductivity in graphene. A positive Lorentzian conductivity may originate from the excitation of plasmons [34]. Terahertz surface plasmons have been predicted theoretically [35, 36], and recently observed in spatially confined graphene [37]. However, the peak frequency of a plasmon dependent conductivity varies with carrier concentration as $\omega_0 \propto n^{1/4}$ [37] and $\text{Re}(\Delta\sigma)$ is expected to be positive, in contrast to our experiments. Figure 2 demonstrates that our measured ω_0 does not decrease with time after photoexcitation, and hence is independent of photoexcited carrier concentration. Additional measurements showed ω_0 to be independent of pump fluence (see Supplementary Discussion). Thus it is unlikely that excitation of plasmons explains the Lorentzian response. A negative photoconductivity may also be attributed to a photo-induced reduction in conductivity, for example by an increase in the carrier-carrier or carrier-phonon (intraband) scattering rates. However it is not clear why such mechanisms would produce a Lorentzian form, or occur only in gas adsorbed graphene. Finally, ground-state bleaching could lead to a negative photoconductivity with Lorentzian form, however the states associated with the absorption of (1.55 eV) optical photons in graphene are well separated from the states near the Dirac point that are associated with interband terahertz absorption and emission (see the inset of Figure 3). We therefore conclude that the opening of a small band gap in the presence of adsorbed gas molecules is the most likely explanation for our measurements.

In summary, we have used terahertz time domain spectroscopy to noninvasively probe photoexcited carrier dynamics in CVD grown graphene. We have observed that gas adsorption can dramatically alter the high frequency electrical response of graphene sheets. We also provide experimental evidence for stimulated emission of terahertz photons in graphene. Furthermore our results demonstrate the huge influence environmental factors can exert on the behaviour of hot carriers in CVD graphene, and highlight the importance of consideration of such factors for future CVD graphene opto-electronic devices.

Methods

Synthesis and Transfer of CVD Graphene

Large-area graphene films were prepared by chemical vapour deposition on 25 μm copper foil (Alfa Aesar). Prior to the growth, the copper foil was heated in hydrogen from room temperature to 1000 °C for 60 minutes for removal of surface oxides. As temperature reached 1000 °C, a mixed flow of H₂ (15 sccm) and

CH₄ (60 sccm) was introduced for graphene growth. After CVD, the graphene film was separated from copper foil and then attached to the z-cut quartz substrate by the polymer transfer process: Poly(methyl methacrylate) (MicroChem Co., NANO PMMA 950K A4) was spin-coated on graphene/copper foil to form a protective layer. The copper foil was etched at 25 °C in ferric nitride solution (50 g/L, J.T.Baker ACS reagent, 98%), leaving a transparent PMMA/graphene film floating on the solution. After rinsing, the film was transferred onto the quartz substrate, and the PMMA capping layer was dissolved in acetone at 60 °C overnight. In order to remove the residual PMMA, graphene films were annealed at 450 °C at 500 Torr in the mixed gases of H₂ (20 sccm) and Ar (80 sccm) for decomposition of the polymer.

Characterisation

Primary characterisation of the sample was performed by Raman spectroscopy [21], using a NT-MDT confocal Raman microscopic system (laser wavelength 473 nm, power 0.5-1 mW, spot size 0.5 μm).

Additional characterisation was performed using UV-visible absorption spectroscopy (Perkin-Elmer Lambda 9 UV-visible- NIR Spectrophotometer) in the range 500-1300 nm, confirming the expected constant $\pi\alpha$ absorption of a single layer of graphene in this wavelength range [22].

Nominally identical samples were characterised using atomic force microscopy (Veeco Dimension-Icon) and room temperature Hall effect measurements based on the Van der pawl method (3S Co., NI PXI-1033). From the Hall effect measurements averaged across 8 samples, the sheet resistance, carrier density and Hall mobility were found to be $1100 \pm 350 \Omega/\square$, $8 \pm 2 \times 10^{12} \text{ cm}^{-2}$ and $800 \pm 250 \text{ cm}^2/\text{Vs}$ respectively. The characterizations show that the quality of the graphene samples is fairly good.

Further Hall effect measurements were performed to examine the equilibrium electrical properties of the graphene samples under different gaseous environments. Two systems were used for the measurements, one based on a permanent magnet (0.68 T), and another using a swept electromagnet (0 – 0.91 T). Samples were held in a vacuum vessel, which could be purged with different gasses. The Fermi levels were deduced using the relation $\varepsilon_F = \hbar v_F \sqrt{\pi n}$, where $v_F \approx 10^6 \text{ ms}^{-1}$ [2, 37].

The equilibrium carrier density, and hence Fermi level, were found to be relatively insensitive to the gaseous environment, with variations in n and ε_F between samples being greater than changes induced by the gases. It was found that, compared with vacuum conditions, exposure to pure nitrogen gas decreased the carrier density by ~ 5%, exposure to oxygen increased the carrier density by ~ 7% and exposure to air increased it by ~ 3%, corresponding to Fermi level changes of ~ 2%, ~ 3% and ~ 1% respectively. These changes are consistent with previous observation of oxygen and nitrogen exposure doping

CVD graphene p-type and n-type respectively [27, 38].

Terahertz spectroscopy

A Ti:sapphire regenerative amplifier (Spectraphysics Spitfire Pro) was used as the pulse laser source for both terahertz generation and optical pumping of the sample: 800 nm, 45 fs pulse duration, 5 kHz repetition rate, 4 W average power. 2.9 W of this beam, reduced to 0.29 W with an neutral density filter, was used to photoexcite the graphene sample, with a maximum fluence of $180 \mu\text{J}/\text{cm}^2$ incident upon the sample, and beam width 2 mm.

A fraction (200 μJ per pulse) of the amplifier beam was used to generate the terahertz probe beam by optical rectification [24] in a 2 mm GaP crystal. The terahertz beam had a width of 0.48 mm at the sample position. The area of graphene probed by the terahertz beam was much smaller than the area photoexcited by the pump beam, thus the probe measured an area of roughly constant photoexcited carrier density.

The remainder of the amplifier beam (16 μJ per pulse) was used as a gate beam for electro-optic sampling [24] of the terahertz field in a 200 μm GaP crystal. The terahertz electric field, E_{THz} , was detected by a balanced photodiode circuit, and the signal extracted using a lock-in amplifier (Stanford Research SR830), referenced to a 2.5 kHz chopper in the terahertz generation beam. A further lock-in (SR830) was used to detect the optical pump induced change in E_{THz} , ΔE , by referencing to a 125 Hz chopper in the sample pump beam.

The gaseous atmospheres used in the terahertz measurements were ambient air, 99.998% pure oxygen free N₂ and 99.99% pure O₂. A vacuum of 10^{-5} mbar, generated using an oil-free pumping system (turbo molecular pump and scroll pump), was used both for the vacuum measurements, and to remove adsorbants from the sample before gaseous measurements.

Acknowledgements

The authors would like to thank the EPSRC (UK) for financial support.

Author Contributions

CJD performed the THz measurements and data analysis. CTL and LJL grew and processed the graphene samples and performed Raman spectroscopy. CJD, HJJ and RJN performed Hall measurements in Oxford. CTL and LJL performed Hall measurements in Taipei. MBJ conceived the study, while all authors discussed the results. CJD and MBJ wrote the manuscript supported by LMH and RJN.

Competing financial interests

The authors declare that they have no competing financial interests.

-
- [1] K S Novoselov, A K Geim, S V Morozov, D Jiang, Y Zhang, S V Dubonos, I V Grigorieva, and A A Firsov. Electric field effect in atomically thin carbon films. *Science*, **306**, 666–669 (2004).
- [2] K S Novoselov, A K Geim, S V Morozov, D Jiang, M I Katsnelson, I V Grigorieva, S V Dubonos, and A A Firsov. Two-dimensional gas of massless dirac fermions in graphene. *Nature*, **438**, 197–200 (2005).
- [3] A K Geim. Graphene: status and prospects. *Science*, **324**, 1530–1534 (2009).
- [4] Q Bao and K P Loh. Graphene Photonics, Plasmonics, and Broad Optoelectronic Devices. *ACS Nano*, **6**, 3677–3694 (2012).
- [5] S Bae, H Kim, Y Lee, X F Xu, J S Park, Y Zheng, J Balakrishnan, T Lei, H R Kim, Y I Song, Y J Kim, K S Kim, B Ozyilmaz, J H Ahn, B H Hong, and S Iijima. Roll-to-roll production of 30-inch graphene films for transparent electrodes. *Nat. Nanotechnol.*, **5**, 574–578 (2010).
- [6] Y M Lin, K A Jenkins, A Valdes-garcia, J P Small, D B Farmer, and P Avouris. Operation of graphene transistors at gigahertz frequencies. *Nano Lett.*, **9**, 422–426 (2009).
- [7] Y Q Wu, Y M Lin, A A Bol, K A Jenkins, F N Xia, D B Farmer, Y Zhu, and P Avouris. High-frequency, scaled graphene transistors on diamond-like carbon. *Nature*, **472**, 74–78 (2011).
- [8] Y M Lin, A Valdes-garcia, S J Han, D B Farmer, I Meric, Y N Sun, Y Q Wu, C Dimitrakopoulos, A Grill, P Avouris, and K A Jenkins. Wafer-scale graphene integrated circuit. *Science*, **332**, 1294–1297 (2011).
- [9] X S Li, W W Cai, J H An, S Kim, J Nah, D X Yang, R Piner, A Velamakanni, I Jung, E Tutuc, S K Banerjee, L Colombo, and R S Ruoff. Large-area synthesis of high-quality and uniform graphene films on copper foils. *Science*, **324**, 1312–1314 (2009).
- [10] H N Wang, J H Strait, P A George, S Shivaraman, V B Shields, M Chandrashekhara, J Hwang, F Rana, M G Spencer, C S Ruiz-vargas, and J Park. Ultrafast relaxation dynamics of hot optical phonons in graphene. *Appl. Phys. Lett.*, **96**, 081917 (2010).
- [11] M B Klarskov, H F Dam, D H Petersen, T M Hansen, A Lowenborg, T J Booth, M S Schmidt, R Lin, P F Nielsen, and P Boggild. Fast and direct measurements of the electrical properties of graphene using micro four-point probes. *Nanotechnology*, **22**, 445702 (2011).
- [12] C J Docherty and M B Johnston. Terahertz properties of graphene. *Journal of Infrared, Millimeter and Terahertz Waves*, **33**, 797–815 (2012).
- [13] J M Dawlaty, S Shivaraman, M Chandrashekhara, F Rana, and M G Spencer. Measurement of ultrafast carrier dynamics in epitaxial graphene. *Appl. Phys. Lett.*, **92**, 042116 (2008).
- [14] P J Hale, S M Hornett, J Moger, D W Horsell, and E Hendry. Hot phonon decay in supported and suspended exfoliated graphene. *Phys. Rev. B*, **83**, 121404 (2011).
- [15] P A George, J Strait, J Dawlaty, S Shivaraman, M Chandrashekhara, F Rana, and M G Spencer. Ultrafast optical-pump terahertz-probe spectroscopy of the carrier relaxation and recombination dynamics in epitaxial graphene. *Nano Lett.*, **8**, 4248–4251 (2008).
- [16] J H Strait, H N Wang, S Shivaraman, V Shields, M Spencer, and F Rana. Very slow cooling dynamics of photoexcited carriers in graphene observed by optical-pump terahertz-probe spectroscopy. *Nano Lett.*, **11**, 4902–4906 (2011).
- [17] H Choi, F Borondics, D A Siegel, S Y Zhou, M C Martin, A Lanzara, and R A Kaindl. Broadband electromagnetic response and ultrafast dynamics of few-layer epitaxial graphene. *Appl. Phys. Lett.*, **94**, 172102 (2009).
- [18] H Y Hwang, N C Brandt, F Hootan, A L Hsu, J Kong, and K A Nelson. Nonlinear thz conductivity dynamics in cvd-grown graphene. Preprint at arXiv:1101.4985 (2011).
- [19] J Horng, C F Chen, B S Geng, C Girit, Y B Zhang, Z Hao, H A Bechtel, M Martin, A Zettl, M F Crommie, Y R Shen, and F Wang. Drude conductivity of dirac fermions in graphene. *Phys. Rev. B*, **83**, 165113 (2011).
- [20] C Lee, J Y Kim, S Bae, K S Kim, B H Hong, and E J Choi. Optical response of large scale single layer graphene. *Appl. Phys. Lett.*, **98**, 071905 (2011).
- [21] A C Ferrari, J C Meyer, V Scardaci, C Casiraghi, M Lazzeri, F Mauri, S Piscanec, D Jiang, K S Novoselov, S Roth, and A K Geim. Raman spectrum of graphene and graphene layers. *Phys. Rev. Lett.*, **97**, 187401 (2006).
- [22] R R Nair, P Blake, A N Grigorenko, K S Novoselov, T J Booth, T Stauber, N M R Peres, and A K Geim. Fine structure constant defines visual transparency of graphene. *Science*, **320**, 1308 (2008).
- [23] A Gupta, G Chen, P Joshi, S Tadigadapa, and P C Eklund. Raman scattering from high-frequency phonons in supported n-graphene layer films. *Nano Lett.*, **6**, 2667–2673 (2006).
- [24] R Ulbricht, E Hendry, J Shan, T F Heinz, and M Bonn. Carrier dynamics in semiconductors studied with time-resolved terahertz spectroscopy. *Rev. Mod. Phys.*, **83**, 543–586 (2011).
- [25] D Grischkowsky, S Keiding, M van Exter, and C Fattinger. Far-infrared time-domain spectroscopy with terahertz beams of dielectrics and semiconductors. *J. Opt. Soc. Am. B-Opt. Phys.*, **7**, 2006–2015 (1990).
- [26] V Ryzhii, M Ryzhii, and T Otsuji. Negative dynamic conductivity of graphene with optical pumping. *J. Appl. Phys.*, **101**, 083114 (2007).
- [27] Y M Shi, W J Fang, K K Zhang, W J Zhang, and L J Li. Photoelectrical response in single-layer graphene transistors. *Small*, **5**, 2005–2011 (2009).
- [28] J Ito, J Nakamura and A Natori. Semiconducting nature of the oxygen-adsorbed graphene sheet. *J. Appl. Phys.*, **103**, 113712 (2008).
- [29] J Berashevich and T Chakraborty. Tunable band gap and magnetic ordering by adsorption of molecules on

- graphene. *Phys. Rev. B*, **80**, 033404 (2009).
- [30] J Y Dai and J M Yuan. Adsorption of molecular oxygen on doped graphene: atomic, electronic, and magnetic properties. *Phys. Rev. B*, **81**, 165414 (2010).
- [31] T Ando. The electronic properties of graphene and carbon nanotubes. *NPG Asia Mater.*, **1**, 17-21 (2009).
- [32] S Ryu, L Liu, S Berciaud, Y J Yu, H T Liu, P Kim, G W Flynn and L E Brus. Atmospheric oxygen binding and hole doping in deformed graphene on a SiO₂ substrate. *Nano Lett.*, **10**, 4944–4951 (2010).
- [33] Y Sato, K Takai and T Enoki . Electrically Controlled Adsorption of Oxygen in Bilayer Graphene Devices. *Nano Lett.*, **11**, 3468-3475 (2011).
- [34] P Parkinson, H J Joyce, Q Gao, H H Tan, X Zhang, J Zou, C Jagadish, L M Herz, and M B Johnston. Carrier lifetime and mobility enhancement in nearly defect-free core-shell nanowires measured using time-resolved terahertz spectroscopy. *Nano Lett.*, **9**, 3349–3353 (2009).
- [35] F Rana. Graphene terahertz plasmon oscillators. *IEEE Trans. Nanotechnol.*, **7**, 91–99 (2008).
- [36] V Ryzhii, A Satou, and T Otsuji. Plasma waves in two-dimensional electron-hole system in gated graphene heterostructures. *J. Appl. Phys.*, **101**, 024509 (2007).
- [37] L Ju, B S Geng, J Horng, C Girit, M Martin, Z Hao, H A Bechtel, X G Liang, A Zettl, Y R Shen, and F Wang. Graphene plasmonics for tunable terahertz metamaterials. *Nat. Nanotechnol.*, **6**, 630–634 (2011).
- [38] B K Daas, W K Nomani, K M Daniels, T S Sudarshan, G Koley, and M V S Chandrashekar. Molecular Gas Adsorption Induced Carrier Transport Studies of Epitaxial Graphene using IR Reflection Spectroscopy. *arXiv:1201.4746v1* (2012).